*Korean J. Chem. Eng.*, **28**(4), 1133-1138 (2011)
DOI: 10.1007/s11814-011-0036-2

# X-ray photoelectron spectroscopic characterization of molybdenum nitride thin films

**Jeong-Gil Choi**†

Department of Nano-Bio Chemical Engineering, HannamUniversity, 461-6 Junmin-dong, Yusung-gu, Daejeon 305-811, Korea
(*Received 22 December 2010 • accepted 15 February 2011*)

**Abstract**−The elemental composition and chemical states of a series of Mo nitride thin films have been investigated using x-ray photoelectron spectroscopy (XPS). The chemical composition and stoichiometry of the films were also tracked as a function of the preparative parameters: the nitrogen ion dose, ion accelerating energy and substrate temperature. At the lowest ion dose, the Mo concentration increased to a depth of ~300 Å. The nitrogen concentration in the film decreased with increasing the ion energy. An increase in the ion energy to 100 and 200 kV led to a lower N/Mo ratio as compared to that at 50 kV. The magnitude of the binding energy separation at room temperature was smaller than that at higher temperatures. This difference might be due to the presence of B1-MoN at higher temperatures and the existence of $\delta$-MoN at lower temperatures.

Key words: Molybdenum Nitride Thin Films, Ion Dose, Ion Energy, Target Temperature

## INTRODUCTION

There has been increasing interest in the preparation of high surface area metal nitrides and carbides since these materials can be used as catalysts and/or catalyst supports [1-4]. Molybdenum nitrides in particular have received a great deal of attention due to their competitive activities for reactions including hydrodenitrogenation [3-5] and $NH_3$ synthesis [6,7]. The catalytic and adsorptive properties of nitrides are governed by their bulk and surface structure and stoichiometry. While there is some information concerning the effects of bulk composition on the catalytic properties of these materials, there is currently very little known about the effects of surface structure and stoichiometry. For this reason, our research uses a series of Mo nitride thin films to derive fundamental relationships between the structure and function of these materials.

In the previous paper we discussed the use of $N^+$ ion implantation to synthesize Mo nitride thin films and investigated the effects of synthesis condition on the formation of Mo nitrides [8]. It has been implied that the electronic and atomic structures of Mo thin films implanted with nitrogen ions are influenced by the ion dose, the ion energy and the substrate temperature [8]. Nevertheless, the effects of these experimental parameters on the electronic structure of Mo nitride thin films have not been systematically elucidated. Our aim here was to investigate the elemental composition and chemical states of Mo nitride thin films using x-ray photoelectron spectroscopy (XPS). In the future these results might be utilized in the understanding of the fundamental relationship between surface properties and catalytic reactivities of these materials. We tracked the chemical composition and stoichiometry of the thin films as a function of the preparative parameters: the nitrogen ion dose, ion accelerating energy and substrate temperature.

†To whom correspondence should be addressed.
E-mail: choi1002@hotmail.com

## EXPERIMENTAL

The deposition and implantation procedures were previously given [8]. The following is to summarize these procedures. Molybdenum thin films were sputter-deposited onto a (100) Si substrate to a thickness of 1,000 Å. The films were then irradiated with nitrogen ions ($N^+$) using 400 kV DL-300Varian ion implanter. The ion beam direction was normal to the substrate surface. The nitrogen ion doses were $4\times10^{16}$, $2\times10^{17}$ and $4\times10^{17}$ $N^+/cm^2$, and the ion accelerating energies were 50, 100 and 200 kV. The nitrogen ion range in Mo was estimated to be 50 to 350 nm based on simulations using the TRIM code program. The nitrogen ion current density ranged from 3.3 to 8.0 $mA/cm^2$. These experimental conditions resulted in a target temperature between room temperature and 773 K. The temperature was measured with a thermocouple attached to the front surface of the substrates.

X-ray photoelectron spectroscopy studies were carried out by using an ESCA PHI5400 spectrometer with Mg-Ka x-ray radiation and a hemispherical electron energy analyzer. The base pressure in the analyzer chamber of the spectrometer was less than $3\times10^{-9}$ torr. The nominal analysis region was about 1.2 mm in diameter. Spectra were collected before and after the samples were sputter-cleaned with $Ar^+$ ions. The sputtering was usually conducted at 3 keV with a current of 10 mA rastering over an area 2.5×2.5 mm. The sputtering rate was estimated to be about 15 Å/min based on the sputtering yield of 1.28 (for Mo sputtered by 3 kV $Ar^+$ ions) and a current density of 1.6 $A/cm^2$. The binding energies were calibrated using Au $4f_{7/2}$=84.0 eV and Cu $2p_{2/2}$=923.6 eV standards. There was always adventitious carbon adsorbed on the sample surface. Charging effects were corrected for by using the binding energy of this adventitious carbon (284.8 eV). The broad envelopes in the Mo $3d_{5/2}$ spectra were deconvoluted to estimate the distribution of the Mo oxidation states (elemental Mo, $Mo^{4+}$, and $Mo^{+6}$). Quantitative relationships between Mo and N (N/Mo atomic ratio) were calculated

from peak area ratios of the respective states in the deconvoluted Mo $3p_{3/2}$ spectra. These areas were normalized by using the atomic sensitivity factors. The relative amounts of carbon and oxygen were also determined based on comparisons of their intensities and atomic sensitivity factors.

## RESULTS AND DISCUSSION

### 1. Effect of Ion Dose

In this section, we consider the effect of varying the nitrogen ion dose with the ion energy and target temperature maintained at 50 kV and 298 K, respectively. Depth profiles for molybdenum, nitrogen, silicon, oxygen and carbon were determined by the alternate collection of XPS spectrum after Ar+ ion sputtering. Figs. 1-3 show the atomic depth distribution following doses of $4\times10^{16}$, $2\times10^{17}$ and $4\times10^{17}$ $N^+/cm^2$, respectively. For all the films, the surfaces of the unsputtered films contained significant amounts of carbon and oxygen. The high concentration of oxygen at the surface is presumably due to surface oxidation following exposure to air. The carbon and oxygen signals decreased significantly after 1 minute of sputtering but remained as minor impurities (<5 at%) throughout the film. The low and constant levels of carbon and oxygen after sputtering were possibly due to the presence of impurities during the Mo deposition process. During deposition the pressure in the chamber was in the range of about $10^{-5}$ torr. In addition, the Si substrate surface almost certainly contained oxygen and carbon before Mo was deposited. It was also expected that adventitious impurities such as carbon were collected on the surface during XPS spectrum collection. Carbon and oxygen are generally difficult to remove completely by ion bombardment cleaning [9]. Thus, small levels of these residual contaminants were expected.

For the films implanted to $2\times10^{17}$ and $4\times10^{17}$ $N^+/cm^2$, the Mo concentration decreased. This latter behavior is due to ion beam mixing between the deposited Mo film and the Si substrate during

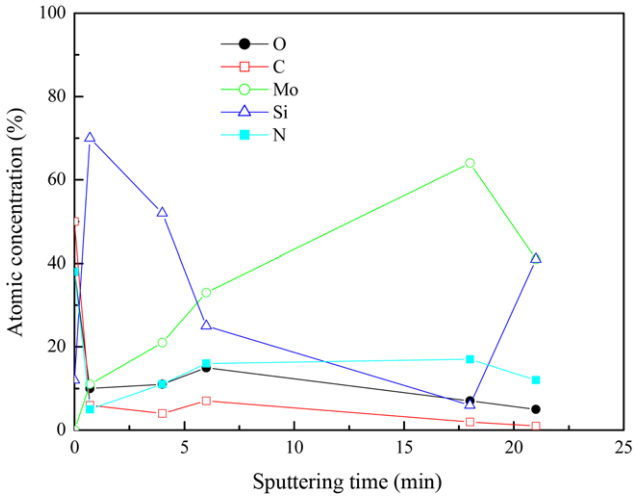


**Fig. 1. Atomic distribution as a function of depth in the nitrogen ion-implanted Mo thin film deposited on Si substrate with $4\times10^{16}$ $N^+/cm^2$ at room temperature and 50 kV.**

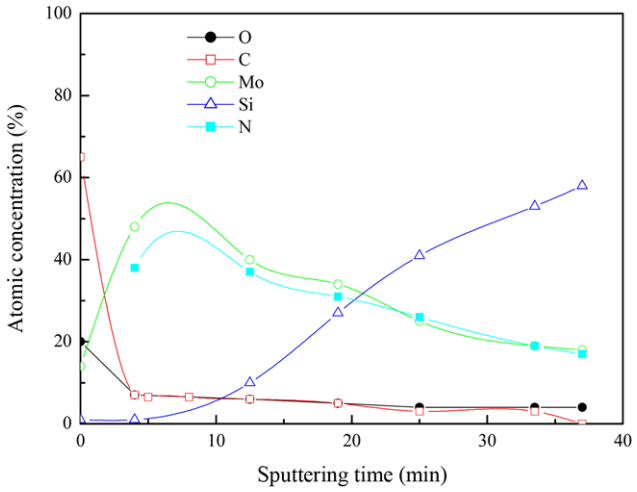


**Fig. 2. Atomic distribution as a function of depth in the nitrogen ion-implanted Mo thin film deposited on Si substrate with $2\times10^{17}$ $N^+/cm^2$ at room temperature and 50 kV.**

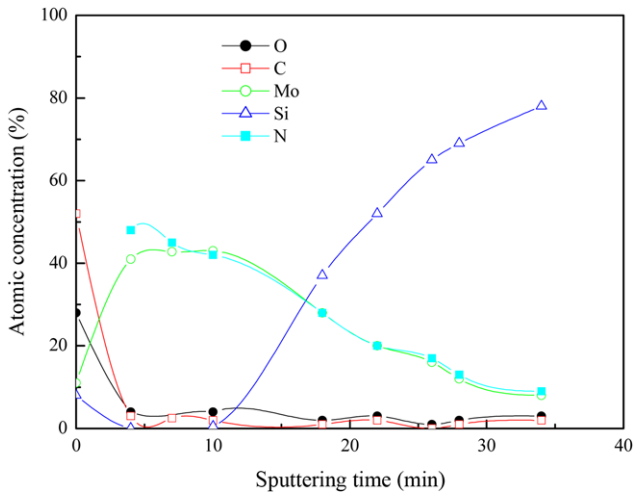


**Fig. 3. Atomic distribution as a function of depth in the nitrogen ion-implanted Mo thin film deposited on Si substrate with $4\times10^{17}$ $N^+/cm^2$ at room temperature and 50 kV.**

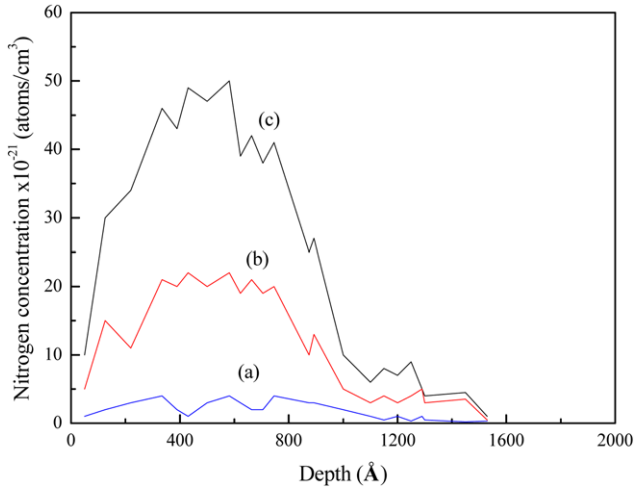


**Fig. 4. Predicted nitrogen depth profiles as a function of ion dose using TRIM program: (a) $4\times10^{16}$ $N^+/cm^2$; (b) $2\times10^{17}$ $N^+/cm^2$; (c) $4\times10^{17}$ $N^+/cm^2$.**

$N^+$ implantation. The film implanted to a dose of $4\times10^{16}$ $N^+/cm^2$ showed a different behavior. The Si concentration was highest near the surface. This behavior is not well understood at this point. In general, the depth profile for an implanted species is expected to be Gaussian, particularly at low doses (10). Nitrogen depth profiles predicted from TRIM code runs are given in Fig. 4. The concentrations of nitrogen implanted at $4\times10^{16}$, $2\times10^{17}$ and $4\times10^{17}$ $N^+/cm^2$ as a function of depth are shown in Fig. 5. The difference between Fig. 4 and 5 is probably due to the assumptions for TRIM runs that no preferential sputtering occurred and stopping conditions did not change during implantation. At $4\times10^{16}$ $N^+/cm^2$ in Fig. 5, the concentration of implanted nitrogen increased to a maximum at a depth of ~150 Å and then decreased. However, the depth profile had a different character for higher nitrogen ion doses. For doses of $2\times10^{17}$ and $4\times10^{17}$ $N^+/cm^2$, the nitrogen concentration was greatest at the surface and decreased with depth. The total area under the nitrogen curves for doses of $2\times10^{17}$ and $4\times10^{17}$ $N^+/cm^2$ was essentially constant. This suggests that at $4\times10^{17}$ $N^+/cm^2$, significant amounts of material were sputtered off the surface. The total area under the nitrogen curve for the low dose was smaller. For all the films, there is no more than 50 at% nitrogen.

The variation of N/Mo atomic ratio with nitrogen ion dose is shown in Fig. 6. At $4\times10^{16}$ $N^+/cm^2$ the estimated N/Mo ratio was about 0.5 through most of the film. This N/Mo ratio is consistent with the XRD results, which suggests the presence of a mixture of $\gamma$-$Mo_2N$ and Mo in the implanted film. As the $N^+$ ion dose was increased, the N/Mo ratios increased substantially to approximately unity and appeared to level off. The N/Mo ratio at $4\times10^{17}$ $N^+/cm^2$ (1.0-1.1) was slightly higher than that at $2\times10^{17}$ $N^+/cm^2$ (0.9-1.0). The XRD results suggested the presence of only $\delta$-MoN at $4\times10^{17}$ $N^+/cm^2$ and showed a mixture of $\gamma$-$Mo_2N$ and Mo at $2\times10^{17}$ $N^+/cm^2$. These observations implied that at $2\times10^{17}$ $N^+/cm^2$, excess nitrogen was dissolved in the lattice during the implantation because the nitrogen dose yielded a higher N/Mo ratio than expected.

Table 1 summarizes the binding energies and relative amounts of Mo in various oxidation states after 4 minutes of sputtering. A 4 minute sputter was used to remove the surface carbon and oxy-

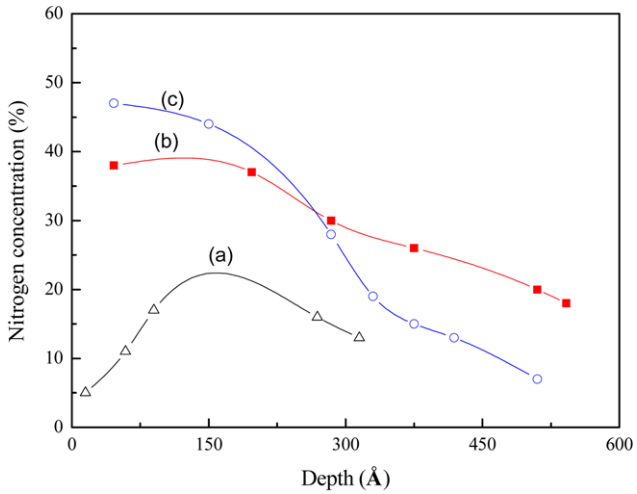


**Fig. 5. Nitrogen concentration depth profiles as a function of ion dose at room temperature and 50 kV: (a) $4\times10^{16}$ $N^+/cm^2$; (b) $2\times10^{17}$ $N^+/cm^2$; (c) $4\times10^{17}$ $N^+/cm^2$.**

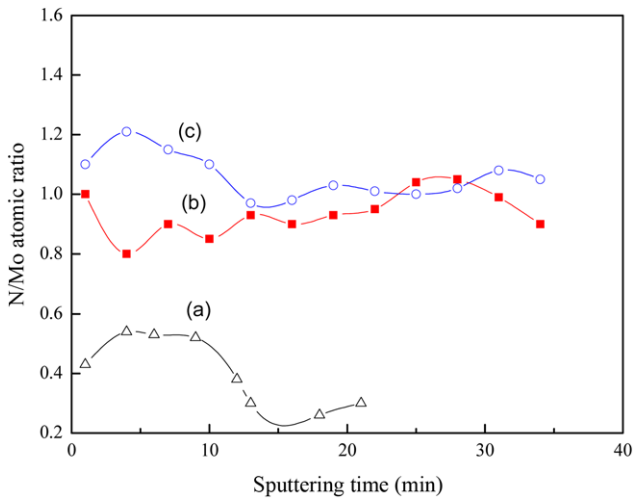


**Fig. 6. Variation of N/Mo atomic ratio as a function of ion dose at room temperature and 50 kV: (a) $4\times10^{16}$ $N^+/cm^2$; (b) $2\times10^{17}$ $N^+/cm^2$; (c) $4\times10^{17}$ $N^+/cm^2$.**

**Table 1. Core level binding energies (eV) for Mo, $Mo^{\delta+}$, $Mo^{4+}$ and $Mo^{6+}$ and their relative amounts after 4 minutes of sputtering**

| Ion dose* ($N^+/cm^2$) | Binding energies (eV) Mo $3d_{5/2}$ | | | |
|---|---|---|---|---|
| | $Mo^0$ | $Mo^{\delta+}$ | $Mo^{4+}$ | $Mo^{6+}$ |
| $4\times10^{16}$ | 227.8 (45)† | 228.7 (38) | 230.0 (17) | - |
| $2\times10^{17}$ | 227.8 (1) | 228.6 (84) | 230.0 (11) | 232.5 (4) |
| $4\times10^{17}$ | 227.8 (3) | 228.7 (83) | 230.1 (10) | 232.5 (4) |

*At room temperature and ion energy of 50 kV

†( )=Percentage based on area intensity from deconvoluted Mo 3d spectra

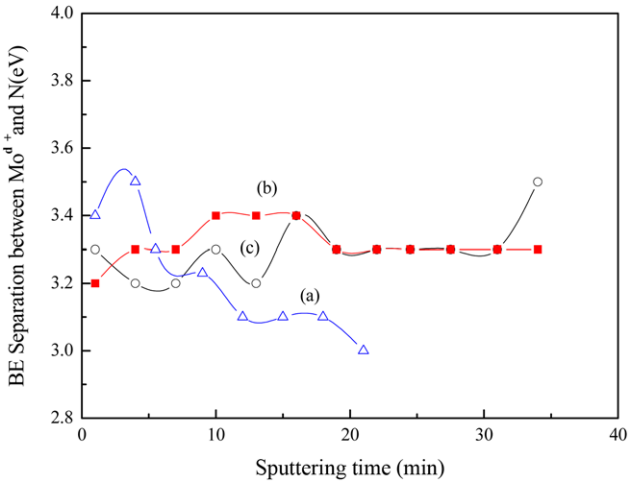


**Fig. 7. Binding energy separation between $Mo^{\delta+}$ and N peaks as a function of ion dose (implantation performed at room temperature and 50 kV): (a) $4\times10^{16}$ $N^+/cm^2$; (b) $2\times10^{17}$ $N^+/cm^2$; (c) $4\times10^{17}$ $N^+/cm^2$.**

gen impurities. Beyond 4 minute sputtering, the binding energies and relative amounts of Mo in various oxidation states were approximately the same within experimental error. In the deconvoluted Mo 3d spectra, the nominal binding energies were 227.8 eV for pure Mo, 228.7 eV for $Mo^{\delta+}$ ($0<\delta<4$), 230.0 eV for $Mo^{4+}$ and 232.5 eV for $Mo^{6+}$. The dominant species appeared to be $Mo^{\delta+}$. Along with the XRD results reported earlier this result supports the proposition that the $Mo^{\delta+}$ peak is due to the formation of Mo nitrides. The $Mo^{\delta+}$ $3p_{3/2}$ peak was located at 394.1 eV (elemental Mo at 393.8 eV) and the N 1s peak was located between 398 and 397.4 eV (peak for adsorbed elemental nitrogen on the surface expected at 398 eV). The amount of $Mo^{4+}$ did not vary significantly with ion dose. The binding energy separation (DE) between the N and $Mo^{\delta+}$ peaks in the thin films is shown in Fig. 7 as a function of ion dose. We believe that the DE between the $Mo^{\delta+}$ $3p_{3/2}$ and N 1s peaks indicates the magnitude of electronic charge transfer between Mo and N in the nitride. Electron charge transfer is expected to occur between the Mo 4d states and N 2p states [11]. The expected DE between elemental Mo and adsorbed nitrogen is 4.2 eV. Since the formation of molysilicide ($MoSi_2$) is not expected below 900 k [11-13], the result suggests that the change in DE following $N^+$ implantation was due to a reaction between Mo and N. Saito et al. [14] reported that the binding energy shift was positive for the Mo 3p level and was negative for the N1s level, indicating the electronic charge transfer occurred from Mo atoms to N atoms. Our results are in good agreement with those of Saito et al. [14].

**2. Effect of Ion Energy**

The depth profile of the implanted nitrogen as well as the projected $N^+$ range was predicted by using the TRIM program for incoming nitrogen ions of 50, 100 and 200 kV (Fig. 8). The projected range of implanted nitrogen and thickness sputtered following a dose of $4\times10^{17}$ $N^+/cm^2$ were estimated using the calculated sputtering yields. The projected range of nitrogen depended on the ion energy used. These predictions are summarized in Table 2.

Fig. 9 shows the measured nitrogen depth profile as a function of ion energy. At an ion energy of 50 kV, the maximum level of the implanted nitrogen was within about 50 Å of the surface, which is much less than the calculated projected $N^+$ range of 566 Å. This

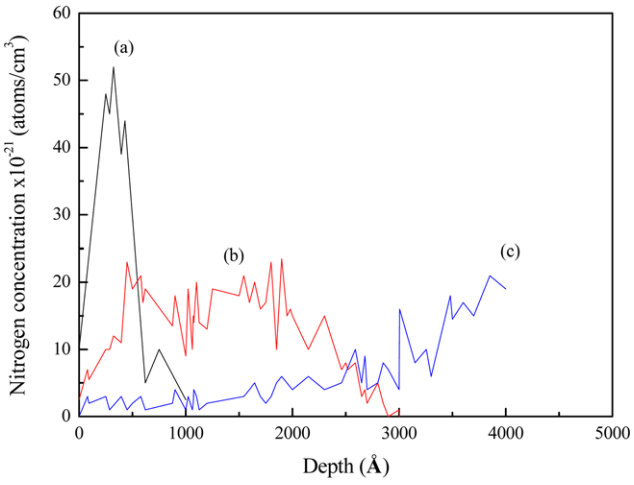


**Fig. 8. Nitrogen depth profiles as a function of ion energy using TRIM program: (a) 50 kV; (b) 100 kV; (c) 200 kV.**

**Table 2. Calculated projected range of implanted nitrogen and sputtered thickness predicted using TRIM-run code based on a dose of $4\times10^{17}$ $N^+/cm^2$**

| Ion energy (kV) | Projected range (Å) | Sputtering yield (atoms/ion) | Film thickness sputtered (Å) |
|---|---|---|---|
| 50 | 566 | 0.309 | 192.6 |
| 100 | 1340 | 0.216 | 134.7 |
| 200 | 3224 | 0.127 | 79.2 |

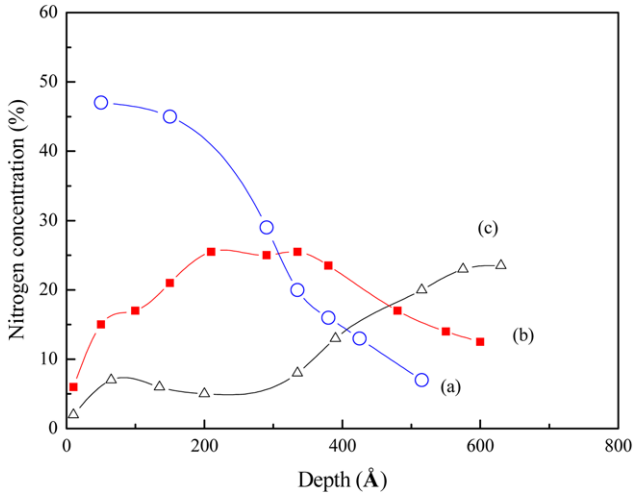


**Fig. 9. Nitrogen concentration depth profile as a function of ion energy at room temperature and $4\times10^{17}$ $N^+/cm^2$: (a) 50 kV; (b) 100 kV; (c) 200 kV.**

suggests that a fair amount of the film surface was sputtered away during irradiation. The thickness of the Mo film sputtered away was estimated to be approximately 500 Å, which is very different from the ~200 Å predicted based on calculations using the TRIM program. Enhanced atomic migration toward the surface at high $N^+$ dose may, to some degree, be responsible for the large deviations. Also, it was assumed in the TRIM program that no preferential sputtering occurs and stopping conditions do not vary during implantation. An increase in the ion energy to 100 kV yielded a range of about 300 Å. In this case, some of the incoming nitrogen was expected to exceed the thickness of the Mo film during implantation. This led to a lower nitrogen concentration in the Mo film as compared to that at 50 kV. At 200 kV, most of the implanted nitrogen penetrated the Mo film into the Si.

Fig. 10 shows the variation of N/Mo atomic ratio as a function of ion energy. At higher ion energies, the N/Mo near the surface was generally lower than that at 50 kV. Up to about 20 minutes of sputtering the average N/Mo ratio at 100 kV was around 0.5. Beyond 20 minute sputtering, the average N/Mo ratio was ~1. The XRD results showed the presence of $\gamma$-$Mo_2N$ and $\gamma$-MoN. At 200 kV, there was very little nitrogen in the Mo film. No Mo nitrides were observed from the XRD results.

The XPS results in terms of ion energy are summarized in Table 3. At 50 kV the majority species was $Mo^{\delta+}$. As ion energy increased up to 200 kV, the relative amount of $Mo^{d+}$ decreased while the amount of elemental Mo increased. The $Mo^{\delta+}$ is only a minor species at 200 kV as compared to elemental Mo. Fig. 11 shows the binding energy

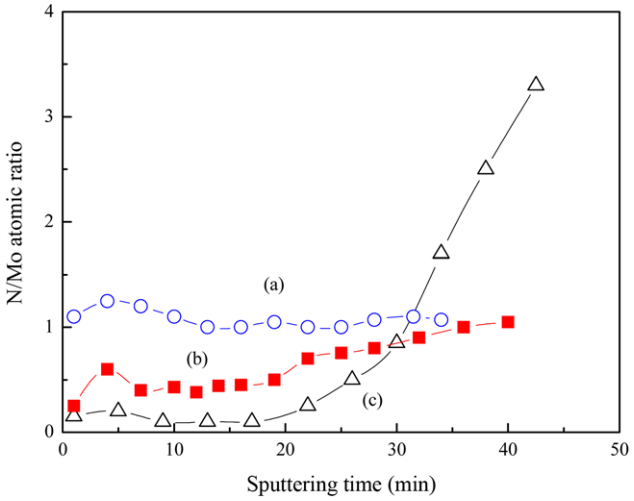


**Fig. 10. Variation of N/Mo atomic ratio as a function of ion energy at room temperature and $4\times10^{17}$ $N^+/cm^2$: (a) 50 kV; (b) 100 kV; (c) 200 kV.**

**Table 3. Core level binding energies (eV) for Mo, $Mo^{\delta+}$, $Mo^{4+}$ and $Mo^{6+}$ and their relative amounts with N/Mo atomic ratio after 4 minutes of sputtering**

| Ion energy* (kV) | Binding energies (eV) Mo $3d_{5/2}$ | | | | N/Mo atomic ratio |
|---|---|---|---|---|---|
| | $Mo^0$ | $Mo^{\delta+}$ | $Mo^{4+}$ | $Mo^{6+}$ | |
| 50 | 227.8 (3)† | 228.7 (82) | 230.0 (10) | 232.5 (5) | 1.16 |
| 100 | 227.8 (34) | 228.6 (56) | 230.0 (10) | - | 0.56 |
| 200 | 227.8 (55) | 228.7 (32) | 230.1 (13) | - | 0.2 |

*At room temperature and $4\times10^{17}$ $N^+/cm^2$

†( )=Percentage based on area intensity from deconvoluted Mo 3d spectra

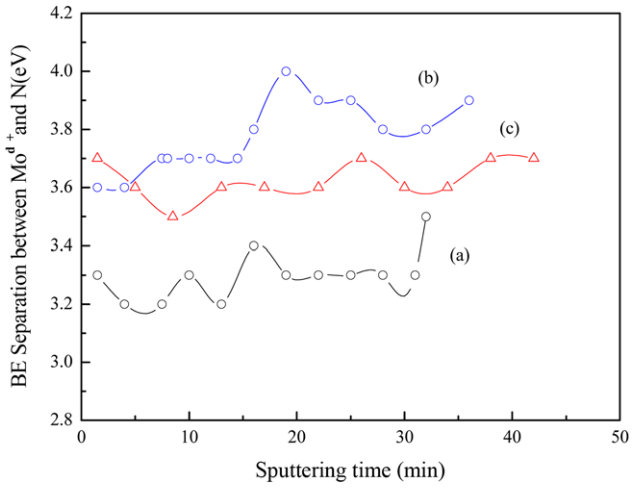


**Fig. 11. Binding energy separation between $Mo^{\delta+}$ and N peaks as a function of ion energy at room temperature and $4\times10^{17}$ $N^+/cm^2$: (a) 50 kV; (b) 100 kV; (c) 200 kV.**

separation between the $Mo^{\delta+}$ and N with various ion energies. The magnitude of DE at 50 kV where only $\delta$-MoN was observed from

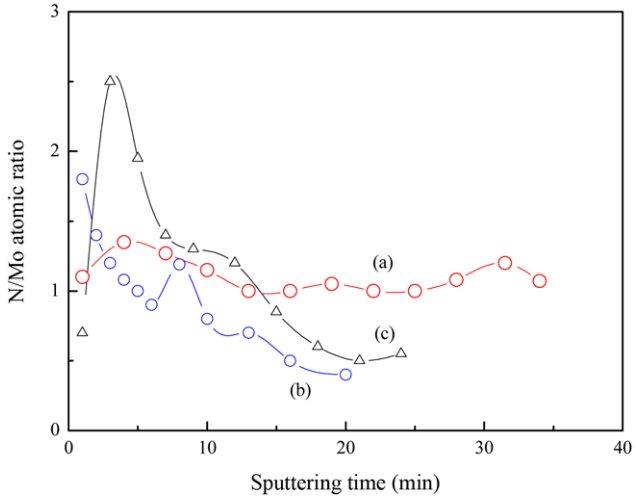


**Fig. 12. Variation of N/Mo atomic ratio as a function of target temperature at $4\times10^{17}$ $N^+/cm^2$ and 50 kV: (a) 298 K (b) 673 K (c) 773 K.**

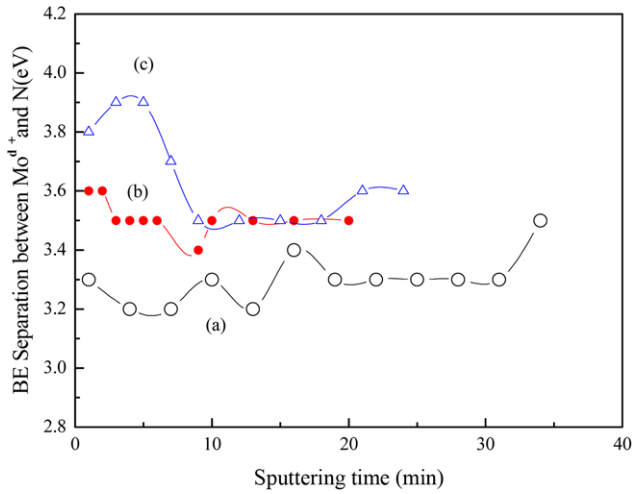


**Fig. 13. Binding energy separation between $Mo^{\delta+}$ and N peaks as a function of target temperature at $4\times10^{17}$ $N^+/cm^2$ and 50 kV: (a) 298 K (b) 673 K (c) 773 K.**

the XRD was smaller than that at 100 kV where a mixture of $\delta$-MoN and $\gamma$-$Mo_2N$ was observed. These results suggest that the degree of electron transfer between Mo and N for $\delta$-MoN is different and smaller than that for $\gamma$-$Mo_2N$ [14]. For catalytic application, Choi et al. [15-17] found that the reaction activity of $\delta$-MoN was much greater than that of $\gamma$-$Mo_2N$ in pyridine hydrodenitrogenation.

### 3. Effect of Target Temperature

One of the most important factors affecting solid state reactions is the temperature (Barrett et al., 1973). In this study, the temperature during implantation was varied from 298 to 773 K. The ion dose was fixed at $4\times10^{17}$ $N^+/cm^2$ and the ion energy was 50 kV.

At target temperatures of 673 and 773 K, there appeared to be an increase in N/Mo ratio near the surface as compared to that at room temperature as shown in Fig. 12. This was profound in the case of the film synthesized at 773 K. For this film, a high N/Mo ratio (2.5) was observed near the surface. The N/Mo ratio subse-

quently decreased gradually with depth. At 673 K, the maximum N/Mo ratio was ~1.8 and the ratio decreased gradually with sputtering. At the higher target temperature the formation of metastable phase B1-MoN along with Mo was observed from the XRD results. It has been reported that nitrides precipitate at the surface at elevated temperatures [18]. Therefore, it was considered that the N/Mo peak near the surface was associated with the precipitation of B1-MoN. The N/Mo ratio decreased with increased sputtering.

Fig. 13 shows the binding energy separation between the implanted N and $Mo^{\delta+}$ as a function of sputtering with various target temperatures. The magnitude of binding energy separation at higher temperature was larger than that at room temperature. This difference is considered to be due to the presence of B1-MoN at higher temperatures and the existence of $\delta$-MoN at lower temperature. Furthermore, the binding energy separation for B1-MoN is larger than that for $\delta$-MoN, suggesting that the degree of electron transfer between Mo and N decreased in the following order: $\gamma$-$Mo_2N$>$\delta$-MoN >B1-MoN.

## CONCLUSION

For all the films, the surfaces of the unsputtered films contained significant amounts of carbon and oxygen. At the lowest ion dose, the Mo concentration increased to a depth of ~300 Å. For the higher ion doses, the Mo concentration increased to a depth of around 150 Å, then decreased gradually while the Si concentration increased. As the ion energy increased, the nitrogen concentration in the Mo film decreased. At 200 kV, most of the implanted was expected to penetrate the Mo film into the Si.

As the target temperature was increased in the temperature range 298-773 K, a nitrogen build up at the surface was observed that is thought to be due to the enhanced nitrogen diffusion and nitride precipitation near the surface at elevated temperatures. This is also considered to be related to the formation of the metastable phase B1-MoN at higher temperatures.

## ACKNOWLEDGEMENTS

This paper has been supported by 2011 Hannam University Research Fund (starting from March 1, 2011 through Feb. 28, 2012).

## REFERENCES

1. J-G. Choi, *J. Kor. Cry. Tech*., **20**, 74 (2010).
2. J-G. Choi, *J. Kor. Cry. Tech*., **20**, 80 (2010).
3. D. J. Sajkowski and S. T. Oyama, *Prep. Petrol. Chem. Div*., 199th ACS Nat. Meeting (1990).
4. S. T. Oyama, J. C. Schlatter, J. E. Metcalfe and J. M. Lambert, *Ind. Eng. Chem. Res*., **27**, 1639 (1988).
5. J.-G. Choi, *J. Ind. Eng. Chem*., **8**, 1 (2002).
6. J.-G. Choi and J.-S. Kim, *J. Ind. Eng. Chem*., **7**, 332 (2001).
7. L. Volpe and M. Boudart, *J. Phys. Chem*., **90**, 4874 (1986).
8. J-G. Choi, D. Choi and L. T. Thompson, *J. Mater. Res*., **7**, 374 (1992).
9. D. Briggs and M. P. Seah, *Practical Surface Analysis by Auger and X-ray Photoelectron Spectroscopy*, Wiley, New York (1983).
10. G. Marest, *Hyperfine Interactions*, **111**, 121 (1998).
11. W-L. Lin, H. Kheyrandish and J. S. Colligon, *Mater. Sci. Eng*., **B1**, 165 (1988).
12. K. S. Grabowski, A. D. F Kahn, E. P. Dovovan and C. A. Carosella, *Nucl. Instr. Meth. Phys. Res*., **B39**, 190 (1989).
13. U. Bussman, F. H. J. Meerbach and E. H. Te Kaat, *Nucl. Instr. Meth. Phys. Res*., **B39**, 230 (1989).
14. K. Saito and Y. Asada, *J. Phys*., **F17**, 2273 (1987).
15. J.-G. Choi, D. Choi and L. T. Thompson, *Appl. Surf. Sci*., **108**, 103 (1997).
16. J.-G. Choi and L. T. Thompson, *Appl. Surf. Sci*., **93**, 143 (1996).
17. J.-G. Choi, J. R. Brenner and L. T. Thompson, *J. Cat*., **154**, 33 (1995).
18. M. Piette, G. Terwagne, W. Moller and F. Bodart, *Mater. Sci. Eng*., **B2**, 189 (1989).